Direct Determination of Band-Gap Renormalization in the Photoexcited Monolayer MoS_2

Fang Liu, Mark E. Ziffer, Kameron R. Hansen, Jue Wang, and Xiaoyang Zhu*
Department of Chemistry, Columbia University, New York, New York 10027, USA

(Received 19 February 2019; published 21 June 2019)

A key feature of monolayer semiconductors, such as transition-metal dichalcogenides, is the poorly screened Coulomb potential, which leads to a large exciton binding energy (E_b) and strong renormalization of the quasiparticle band gap (E_g) by carriers. The latter has been difficult to determine due to a cancellation in changes of E_b and E_g, resulting in little change in optical transition energy at different carrier densities. Here, we quantify band-gap renormalization in macroscopic single crystal MoS_2 monolayers on SiO_2 using time and angle-resolved photoemission spectroscopy. At an excitation density above the Mott threshold, E_g decreases by as much as 360 meV. We compare the carrier density-dependent E_g with previous theoretical calculations and show the necessity of knowing both doping and excitation densities in quantifying the band gap.

DOI: 10.1103/PhysRevLett.122.246803

Atomically thin transition-metal dichalcogenide (TMDC) monolayers and heterojunctions are being broadly explored as model systems for a wide range of electronic, optoelectronic, and quantum processes. The commonly studied TMDC monolayers possess direct band gaps in the visible to near-IR region [1–3]. Because of the strong many-body Coulomb interactions in monolayer TMDCs, both the exciton binding energy (E_b) and band gap renormalization energy are large [3]. The former lowers the optical transition energy by hundreds of milli-electron volts from E_g, while the latter decreases E_g by similar amounts in the presence of charge carriers or excitons. The band-gap renormalization energy (ΔE_g) and decrease in exciton binding energy (ΔE_b) tend to be of similar magnitudes but counteract each other, leading to comparatively modest changes in optical transition energies [4,5]. Since the quasiparticle band gap E_g is the most fundamental quantity and is predicted to be exceptionally sensitive to carrier or exciton densities [4,6,7], there is clearly a need to determine band-gap renormalization and its dependence on carrier and/or exciton densities.

Past attempts at measuring ΔE_g required analysis of subtle or small features in optical spectra [8–11]. Examples include estimating the gain threshold in transient reflectance spectra from photoexcited TMDC monolayers and bilayers above the Mott density [8], extrapolating E_g from the experimental Rydberg exciton series in conjunction with theoretical models [9,10], and identifying features attributed to band-gap transition on the broad fluorescence excitation spectra of gate-doped monolayer MoS_2 [11]. The ideal technique to determine quasiparticle energies is angle-resolved photoelectron spectroscopy (ARPES), which directly maps band energies with momentum resolution. ARPES typically probes the valence bands and populating the conduction band would require either (a) heavy chemical doping via K or H atom deposition [12–15] or (b) photodoping via above-gap optical excitation in time-resolved (TR) ARPES [16–18]. The chemical doping approach may lead to undesirable changes to the dielectric environment and lattice structure of TMDC monolayers [12–15,19]. TR-ARPES of transiently excited TMDCs can in principle probe both the quasiparticle band gap and the dynamics of band-gap renormalization. However, past attempts of TR-ARPES on TMDC monolayers have used CVD grown polycrystalline monolayers on metal or semimetal substrates [16–18]. These conductive substrates drastically modify both the energetics and dynamics of excited states in TMDC monolayers [16–18]. Other TR-ARPES studies have used bulk TMDC crystals, instead of monolayers [20–23]. To overcome these limitations, here we prepare single crystal MoS_2 monolayers with macroscopic sizes (millimeter to centimeter) on dielectric substrates (285 nm thick SiO_2 on n-doped Si). We use TR-ARPES to monitor the time evolution of the valence band maximum (VBM) and conduction band minimum (CBM) following above-gap optical excitation. We directly quantify band-gap energies with excitation density across the Mott threshold and compare experimental results with recent theoretical calculations.

In our femtosecond TR-ARPES experiment [Fig. 1(a) and Fig. S3], the visible excitation pulse ($h\nu_1 = 2.2$ eV, 40 fs pulse width, s polarized) is obtained from a homebuilt noncolinear optical parametric amplifier, pumped by a Ti:sapphire laser (Coherent Legend, 10 W, 10 kHz, 800 nm, 35 fs). Part of the Ti:sapphire laser output is frequency doubled for high harmonic generation in Kr gas (KM Labs, XUUS) to produce EUV probe pulses ($h\nu_2 = 22$ eV, pulse duration <100 fs, p polarized) [24]. The EUV pulse ionizes electrons from both valence and conduction bands for detection by a hemispherical analyzer with angular resolution. Note that the use of EUV, instead UV probe, is necessary to access the high momentum K point at the Brillouin zone corner. The plane of light incidence and analyzer slit is parallel to the Γ-K direction, with the sample azimuthal geometry fixed for the collection of photoemission from the K valley.

Figure 1(b) shows an optical image of a single crystal MoS_2 monolayer (blue color) on the SiO_2/Si substrate. Our improvement to the gold-assisted exfoliation technique [25] has yielded macroscopic single crystal samples (lateral dimension in the millimeter-to-centimeter range). See Figs. S1 and S2 in the Supplemental Material [26] for characterization with atomic force microscope (AFM) for sample cleanness and second harmonic generation (SHG) for alignment of the crystal axis. The complex dielectric function [Fig. 1(c)] obtained from white light reflectance shows the characteristic A and B excitons and photoluminescence spectrum [Fig. 1(d)] shows emission from the A exciton ($E_A = 1.865 \pm 0.05$ eV). These optical spectra are consistent with those of previous reports [1,33].

In the TR-ARPES experiment, the visible pump pulse induces a direct transition in the K and K' valleys. Following a controlled time delay (Δt), the EUV probe pulse ionizes the electrons in the valence and conduction bands. Figure 2 shows momentum-resolved ARPES from monolayer MoS_2 around the K valley without (a) and with (b) the visible pump ($\Delta t = 0$). The two spectra are integrated over the 1.1–1.4 $Å^{-1}$ parallel momentum window to yield the corresponding energy distribution curves (EDCs), shown in Fig. 2(c). The MoS_2 monolayer sample is n doped, with the Fermi energy close to the CBM. As a result, a weak photoelectron signal from the intrinsic population in the conduction band near CBM is observed in Fig. 2(a). This signal is used to determine a doping density of $n_0 = (4.9 \pm 1.0) \times 10^{12}$ cm^{-2} (see Supplemental Material, Fig. S6 [26]). Mechanically exfoliated MoS_2 monolayers are commonly known to be of n type at similar doping levels [34–36].

With the addition of the pump pulse, photoexcitation across the band gap creates exciton and/or electron-hole carrier density $n_{e/h}$ on top of n_0. In the experiment, we vary the excitation densities $n_{e/h}$ in the range of 3.8×10^{12} to 2.3×10^{13} cm^{-2}. For reference, the Mott density for the transition from exciton gas to electron-hole plasma is $n_{\mathrm{Mott}} \sim 4.3 \times 10^{12}$ cm^{-2}, estimated from the 2D scaling relationship [7] of $a_0 n_{\mathrm{Mott}}^{1/2} \approx 0.25$ with a_0 (exciton Bohr radius) = 1.2 nm for undoped monolayer MoS_2 on SiO_2 [37]. The excitation density probed here is mostly in the e-h plasma region. Figure 2(b) shows ARPES spectra at an excitation density of $n_{e/h} = (2.3 \pm 0.5) \times 10^{13}$ cm^{-2} at $\Delta t = 0$. Compared to Fig. 2(a), we observe three major changes: (1) an increase in conduction band

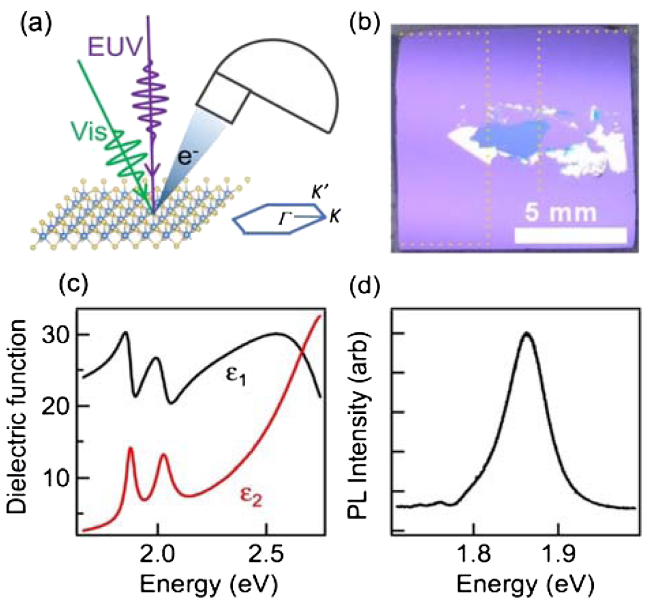

FIG. 1. The macroscopic single crystal MoS_2 monolayer sample and characterization. (a) Schematics of TR-ARPES experiment, combining the femtosecond visible pump (green) and EUV probe (purple). The photoelectrons are collected by the hemispherical analyzer at a specific angle θ from the surface normal, corresponding to emission from a K valley. (b) Image of the single crystal MoS_2 monolayer. We deposit Au films in the dashed areas for electrical contact and grounding. (c) Complex dielectric function ($\varepsilon = \varepsilon_1 + i\varepsilon_2$) of the monolayer MoS_2 determined from reflectance spectroscopy and (d) photoluminescence spectrum of the MoS_2 monolayer at room temperature.

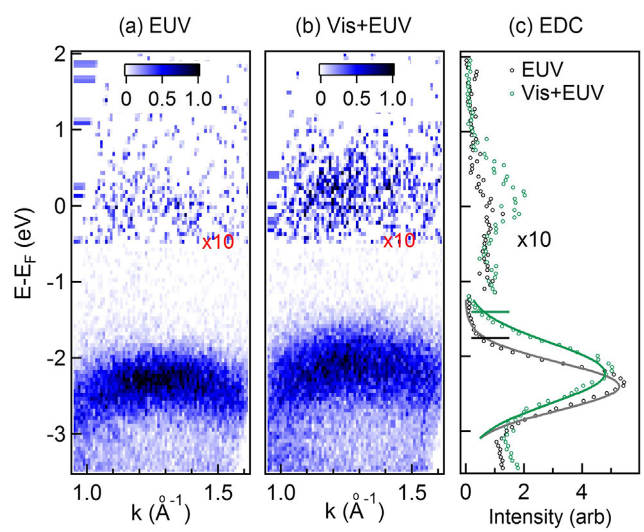

FIG. 2. TR-ARPES from monolayer MoS_2. (a),(b) EUV ARPES of single crystal MoS_2 monolayer without and with the visible pump excitation ($\Delta t = 0$). The APRES spectra is collected at K valley along Γ to K direction. The visible pump is at a photon energy of 2.2 eV. (c) Corresponding electron energy distribution curves (EDC). The solid lines are Gaussian functional fits. The horizontal marks represent the edges of the EDCs, corresponding to $E_0 + 2\sigma$. The spin orbit splitting at K valley is not resolved under the current energy resolution. The excitation density from the pump pulse is $n_{e/h} = (2.3 \pm 0.5) \times 10^{13}$ cm^{-2}. The conduction band signal is magnified by 10× for clarity.

electron intensity; (2) an upshift in the VBM; and (3) a broadening in the valence band EDC. The photoelectron signal from the conduction band at $\Delta t = 0$ probes $n_0 + n_{e/h}$; therefore, the prompt increase in CB photoemission signal, observation (1), is proportional to the excitation density $n_{e/h}$. To understand observations (2) and (3), we point out that the depletion in the valence band by optical excitation is ∼1% of the total electron density in the band and not detectable in our experiment. Thus, the upshift in VBM and broadening of the valence band results from many-body effects resulting from the excitation. The former measures the band renormalization [4,6,7] and the latter is attributed to dephasing from hole-hole scattering [38].

We now turn to the dynamics of the many-body effects following optical excitation. Figures 3(a) and 3(b) are 2D pseudocolor EDC plots showing the conduction band and valence band photoemission signal, respectively, as a function of pump-probe delay Δt. Note that EDC spectra were taken with analyzer energies focused on CB and VB, resulting in a better S/N than that shown in Fig. 2, especially for the CB. A representative EDC at a single time slice is shown in Fig. S5 [26]. Because of the low electron population in the conduction band, we assume these electrons reside close to the CBM and take the intensity-weighted average of the CB photoelectron energies as the CBM position. For the VBM, a common practice in photoemission studies is to use linear extrapolation near the threshold, which may introduce large uncertainty. Instead, each valence band EDC from the K valley is well described by a Gaussian function, and therefore we use the high-energy cutoff at $E_a + 2\sigma$ (E_a is the intensity-weighted average of the valence band energy and σ is variance of the Gaussian fit) to represent the VBM. These two approaches yield similar VBM values, as shown in the Supplemental Material (Fig. S5) [26].

Figure 3(c) shows the VBM-CBM positions as a function of Δt. Interestingly, the photoexcitation induced band-gap renormalization is reflected exclusively in the upshift in the VBM while the CBM remains constant, suggesting that the CBM is pinned to the Fermi level of the metal contact in our n-doped sample, in agreement with Bampoulis *et al.* [34]. The difference between CBM and VBM gives the time-dependent E_g. In the calculation of the band gap, the CBM is fixed at the time-averaged value of 0.223 eV above the Fermi energy. As is shown in Fig. 3(d), E_g is measured to be 2.19 ± 0.10 eV in the absence of optical excitation ($\Delta t < 0$), which is ∼0.4 eV lower than $E_g = 2.6 \pm 0.2$ eV in undoped monolayer MoS_2 [6,11]. This difference reflects band renormalization from the intrinsic n-type doping of $n_0 = (4.9 \pm 1.0) \times 10^{12}$ cm^{-2} [6,11]. At $\Delta t = 0$, photoexcitation across the band gap further lowers E_g by as much as $\Delta E_g = -0.36 \pm 0.04$ eV.

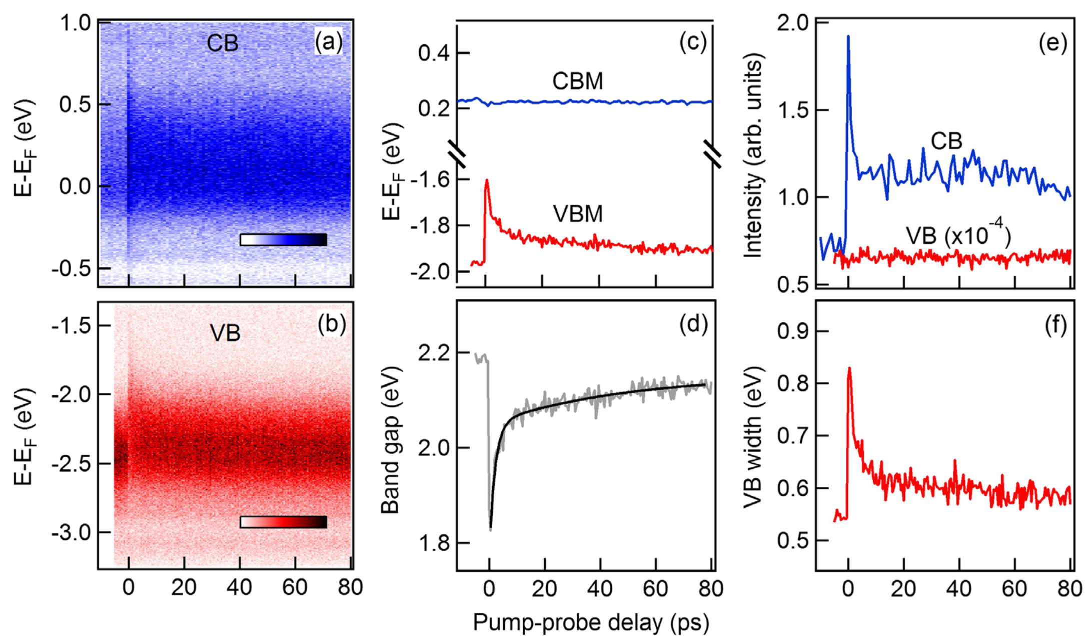

FIG. 3. Dynamics of band renormalization. All panels are shown as a function of pump-probe delay: (a) and (b) are 2D pseudocolor (intensity) plots of EDC spectra collected individually for conduction band and valence band, respectively; (c) CBM and VBM positions extracted from EDC scans shown in panels (a) and (b); (d) band gap E_g (gray) with biexponential fit (black solid line); (e) conduction (blue) and valence (red) band photoelectron intensities; and (f) full width at half maximum of valence band. To obtain the EDCs in (a) and (b), the photoelectron signal is integrated from 1.1 to 1.4 Å^{-1}. The CBM is fixed at the time-averaged value of 0.223 eV in the calculation of the band gap in (d). The initial excitation density is $n_{e/h} = 1.3 \times 10^{13}$ cm^{-2} and the sample is at 295 K. The color scales in (a) and (b) are normalized (0–1).

The large photoinduced band-gap renormalization results from the poorly screened Coulomb potential and strong many-body interactions in the TMDC monolayer. The renormalized band gap, initially by $\Delta E_g = -0.36 \pm 0.04$ eV at $\Delta t = 0$, recovers with increasing Δt due to carrier recombination. This recovery can be described by a biexponential fit [solid curve in Fig. 3(d)], with time constants of $\tau_d = 2$ and 80 ps, respectively. The time dependence in E_g is consistent with the population decay of conduction band photoelectron intensity [blue curve in Fig. 3(e)], as well as in the recovery of valence bandwidth [Fig. 3(f)]. For comparison, the photoelectron intensity from the valence band [red curve in Fig. 3(e)] remains constant, as expected from the small depletion of the valence band (∼1%) due to photoexcitation. At such a high excitation density, the fast decay ($\tau_d = 2$ ps) likely results from Auger recombination [39], while the slow decay can be attributed to intrinsic radiative or nonradiative decays in the MoS_2 monolayer [40]. We point out that electronic interaction with or screening by the SiO_2 dielectric substrate is minimal for our single crystal MoS_2 monolayer and photoexcited carrier populations survive for over 400 ps at room temperature (see Fig. S9). For comparison, previous experiments of polycrystalline TMDC monolayers on metal or graphene substrates show lifetimes up to 4 orders of magnitude shorter [17,18]. Thus, the band renormalization determined here reflects close-to intrinsic many-body interactions in the MoS_2 monolayer [37]. The time-dependent band renormalization quantified in our TR-ARPES measurement is also in qualitative agreement with previous optical measurements on monolayer TMDCs [7,8,11,41–43].

Our ability to determine band-gap renormalization in macroscopic MoS_2 monolayers on an dielectric substrate allows us to carry out quantitative comparisons to theoretical predictions [4,6,7,44]. The solid circles in Fig. 4 are band-gap values determined in our TR-ARPES measurements at different excitation densities. The photoinduced electron-hole density $n_{e/h}$ coexists with the intrinsic electron density of $n_0 = (4.9 \pm 1.0) \times 10^{12}$ cm^{-2} from n-type doping. Both e/h pairs from optical excitation and excess electrons from n-type doping screen the Coulomb interactions, leading to renormalization of the band gap. We use the total carrier density, i.e., $n_0 + 2n_{e-h}$, in comparison to previous calculations for either electron doping or e/h pair excitation. Liang *et al.* calculated band renormalization (red curve) from the quasiparticle self-energies of valence and conduction bands in monolayer MoS_2 using a new plasmon-pole model that takes into account carrier occupation and carrier screening at high electron doping levels [6]. The result is close to that of a more recent *GW* calculation (blue curve) by the same group [44]. Meckbach *et al.* incorporated plasma dielectric screening into a four band Hamiltonian and solved the Dirac-Bloch equation to obtain renormalized band gaps at different excitation densities

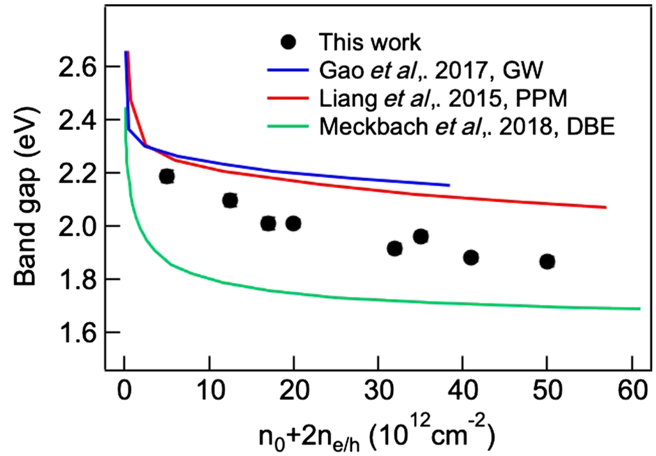

FIG. 4. Comparison of experimental band gaps with theoretical calculations. Solid circles are experimental band gaps for monolayer MoS_2 determined by TR-ARPES as a function of total doping density ($n_0 + 2n_{e/h}$). The solid curves are theoretical results for electron doping (red [6] and blue [44]) or e/h pair generation from optical excitation (green) [7].

($n_{e/h}$) [7]. The resulting band-gap values (green curve) are below those predicted for only electron doping (red and blue curves). While the first data point for $n_0 = (4.9 \pm 1.0) \times 10^{12}$ cm^{-2} in our measurement (without photoexcitation) is very close to the theoretical results for the same electron doping density [6,44], the experiment data points move closer to the results of Meckbach *et al.* for photodoping [7]. This comparison reveals the critical importance of knowing both intrinsic doping levels and additional photoexcitation densities in quantifying the band gap in 2D TMDCs.

In summary, we carry out direct and quantitative measurement of band-gap renormalization in photoexcited MoS_2 monolayers using TR-ARPES. The use of macroscopic and single crystal MoS_2 samples on a dielectric (SiO_2) surface allows us to access the close-to-intrinsic band-gap renormalization and carrier decay dynamics in the 2D semiconductor. We show reduction in the band gap by as much −0.36 eV for photoexcitation above the Mott density in an n-type MoS_2 monolayer. The measured density-dependent band gap provides a benchmark for the validation of theoretical models and for the understanding of strong many-body interactions in TMDC monolayers.

X. Y. Z. acknowledges the National Science Foundation (NSF) Grant No. DMR-1608437 for supporting the TR-ARPES measurements and NSF Grant No. DMR-1809680 for supporting the sample preparation. X. Y. Z. acknowledges the Center for Precision Assembly of Superstratic and Superatomic Solids, a Materials Science and Engineering Research Center (MRSEC) through NSF Grant No. DMR-142063 for supporting the purchase and development of the extreme-UV laser source and for the optical characterization of monolayer MoS_2 samples. Partial support by the Columbia Nano Initiative and the Vannevar Bush Faculty Fellowship through Office of Naval Research Grant No. N00014-18-1-2080 for the purchase of the laser equipment is also acknowledged. This research was supported in part by the Department of Energy (DOE) Office of Energy Efficiency and Renewable Energy (EERE) Postdoctoral Research Award under the EERE Solar Energy Technologies Office administered by the Oak Ridge Institute for Science and Education (ORISE) for the DOE. ORISE is managed by Oak Ridge Associated Universities (ORAU) under DOE Contract No. DE-SC00014664. All opinions expressed in this paper are the author's and do not necessarily reflect the policies and views of DOE, ORAU, or ORISE. We acknowledge Dr. Yusong Bai for help in SHG and PL experiments.

*To whom correspondence should be addressed.
xyzhu@columbia.edu

[1] K. F. Mak, C. Lee, J. Hone, J. Shan, and T. F. Heinz, Phys. Rev. Lett. **105**, 136805 (2010).

[2] A. Splendiani, L. Sun, Y. Zhang, T. Li, J. Kim, C. Y. Chim, G. Galli, and F. Wang, Nano Lett. **10**, 1271 (2010).

[3] G. Wang, A. Chernikov, M. M. Glazov, T. F. Heinz, X. Marie, T. Amand, and B. Urbaszek, Rev. Mod. Phys. **90**, 021001 (2018).

[4] S. Gao, Y. Liang, C. D. Spataru, and L. Yang, Nano Lett. **16**, 5568 (2016).

[5] A. Raja, A. Chaves, J. Yu, G. Arefe, H. M. Hill, A. F. Rigosi, T. Korn, C. Nuckolls, J. Hone, T. C. Berkelbach, P. Nagler, C. Schu, L. E. Brus, T. F. Heinz, D. R. Reichman, and A. Chernikov, Nat. Commun. **8**, 15251 (2017).

[6] Y. Liang and L. Yang, Phys. Rev. Lett. **114**, 063001 (2015).

[7] L. Meckbach, T. Stroucken, and S. W. Koch, Appl. Phys. Lett. **112**, 061104 (2018).

[8] A. Chernikov, C. Ruppert, H. M. Hill, A. F. Rigosi, and T. F. Heinz, Nat. Photonics **9**, 466 (2015).

[9] A. Chernikov, A. M. van der Zande, H. M. Hill, A. F. Rigosi, A. Velauthapillai, J. Hone, and T. F. Heinz, Phys. Rev. Lett. **115**, 126802 (2015).

[10] B. Liu, W. Zhao, Z. Ding, I. Verzhbitskiy, L. Li, J. Lu, J. Chen, G. Eda, and K. P. Loh, Adv. Mater. **28**, 6457 (2016).

[11] K. Yao, A. Yan, S. Kahn, A. Suslu, Y. Liang, E. S. Barnard, S. Tongay, A. Zettl, N. J. Borys, and P. J. Schuck, Phys. Rev. Lett. **119**, 087401 (2017).

[12] T. Eknapakul, P. D. C. King, M. Asakawa, P. Buaphet, R.-H. He, S.-K. Mo, H. Takagi, K. M. Shen, F. Baumberger, T. Sasagawa, S. Jungthawan, and W. Meevasana, Nano Lett. **14**, 1312 (2014).

[13] D. Pierucci, H. Henck, Z. Ben Aziza, C. H. Naylor, A. Balan, J. E. Rault, M. G. Silly, and Y. J. Dappe, ACS Nano **11**, 1755 (2017).

[14] J. Katoch, S. Ulstrup, R. J. Koch, S. Moser, K. M. McCreary, S. Singh, J. Xu, B. T. Jonker, R. K. Kawakami, A. Bostwick, E. Rotenberg, and C. Jozwiak, Nat. Phys. **14**, 355 (2018).

[15] Y. Zhang, T. Chang, B. Zhou, Y.-T. Cui, H. Yan, Z. Liu, F. Schmitt, J. Lee, R. Moore, Y. Chen, H. Lin, H.-T. Jeng, S.-K. Mo, Z. Hussain, A. Bansil, and Z.-X. Shen, Nat. Nanotechnol. **9**, 111 (2014).

[16] S. Ulstrup, A. G. Čabo, D. Biswas, J. M. Riley, M. Dendzik, C. E. Sanders, M. Bianchi, C. Cacho, D. Matselyukh, R. T. Chapman, E. Springate, P. D. C. King, J. A. Miwa, and P. Hofmann, Phys. Rev. B **95**, 041405(R) (2017).

[17] S. Ulstrup, A. G. Čabo, J. A. Miwa, J. M. Riley, S. S. Grønborg, J. C. Johannsen, C. Cacho, O. Alexander, R. T. Chapman, E. Springate, M. Bianchi, M. Dendzik, J. V. Lauritsen, P. D. C. King, and P. Hofmann, ACS Nano **10**, 6315 (2016).

[18] A. Grubišić Čabo, J. A. Miwa, S. S. Grønborg, J. M. Riley, J. C. Johannsen, C. Cacho, O. Alexander, R. T. Chapman, E. Springate, M. Grioni, J. V Lauritsen, P. D. C. King, P. Hofmann, and S. Ulstrup, Nano Lett. **15**, 5883 (2015).

[19] H. Fang, M. Tosun, G. Seol, T. C. Chang, K. Takei, J. Guo, and A. Javey, Nano Lett. **13**, 1991 (2013).

[20] R. Wallauer, J. Reimann, N. Armbrust, J. Güdde, and U. Höfer, Appl. Phys. Lett. **109**, 162102 (2016).

[21] A. Tanaka, N. J. Watkins, and Y. Gao, Phys. Rev. B **67**, 113315 (2003).

[22] R. Bertoni, C. W. Nicholson, L. Waldecker, H. Hübener, C. Monney, U. De Giovannini, M. Puppin, M. Hoesch, E. Springate, R. T. Chapman, C. Cacho, M. Wolf, A. Rubio, and R. Ernstorfer, Phys. Rev. Lett. **117**, 277201 (2016).

[23] P. Hein, A. Stange, K. Hanff, L. X. Yang, G. Rohde, K. Rossnagel, and M. Bauer, Phys. Rev. B **94**, 205406 (2016).

[24] S. Eich, A. Stange, A. V. Carr, J. Urbancic, T. Popmintchev, M. Wiesenmayer, K. Jansen, A. Ruffing, S. Jakobs, T. Rohwer, S. Hellmann, C. Chen, P. Matyba, L. Kipp, K. Rossnagel, M. Bauer, M. M. Murnane, H. C. Kapteyn, S. Mathias, and M. Aeschlimann, J. Electron Spectrosc. Relat. Phenom. **195**, 231 (2014).

[25] S. B. Desai, S. R. Madhvapathy, M. Amani, D. Kiriya, M. Hettick, M. Tosun, Y. Zhou, M. Dubey, J. W. Ager, D. Chrzan, and A. Javey, Adv. Mater. **28**, 4053 (2016).

[26] See Supplemental Material at http://link.aps.org/supplemental/10.1103/PhysRevLett.122.246803, which includes Refs. [27–32], for experimental methods, including (i) the preparation of macroscopic MoS_2 single crystal monolayer; (ii) characterization by reflectance spectroscopy and photoluminescence spectroscopy; and (iii) time-resolved ARPES measurements; also, additional data and analysis.

[27] S. Ulstrup, J. C. Johannsen, F. Cilento, A. Crepaldi, J. A. Miwa, M. Zacchigna, C. Cacho, R. T. Chapman, E. Springate, F. Fromm, C. Raidel, T. Seyller, P. D. C. King, F. Parmigiani, M. Grioni, and P. Hofmann, J. Electron Spectrosc. Relat. Phenom. **200**, 340 (2015).

[28] S.-L. Yang, J. A. Sobota, P. S. Kirchmann, and Z.-X. Shen, Appl. Phys. A **116**, 85 (2014).

[29] M. Alonso, R. Cimino, and K. Horn, Phys. Rev. Lett. **64**, 1947 (1990).

[30] S. Tanaka, J. Electron Spectrosc. Relat. Phenom. **185**, 152 (2012).

[31] L.-P. Oloff, K. Hanff, A. Stange, G. Rohde, F. Diekmann, M. Bauer, and K. Rossnagel, J. Appl. Phys. **119**, 225106 (2016).

[32] H. Wang, C. Zhang, W. Chan, S. Tiwari, and F. Rana, Nat. Commun. **6**, 8831 (2015).

[33] Y. Li, A. Chernikov, X. Zhang, A. Rigosi, H. M. Hill, A. M. van der Zande, D. A. Chenet, E. M. Shih, J. Hone, and T. F. Heinz, Phys. Rev. B **90**, 205422 (2014).

[34] B. Radisavljevic, A. Radenovic, J. Brivio, V. Giacometti, and A. Kis, Nat. Nanotechnol. **6**, 147 (2011).

[35] A. Ayari, E. Cobas, O. Ogundadegbe, and M. S. Fuhrer, J. Appl. Phys. **101**, 014507 (2007).

[36] K. F. Mak, K. He, C. Lee, G. H. Lee, J. Hone, T. F. Heinz, and J. Shan, Nat. Mater. **12**, 207 (2013).

[37] X.-Y. Zhu, N. R. Monahan, Z. Gong, H. Zhu, K. W. Williams, and C. A. Nelson, J. Am. Chem. Soc. **137**, 8313 (2015).

[38] J. Kanasaki, H. Tanimura, K. Tanimura, P. Ries, W. Heckel, K. Biedermann, and T. Fauster, Phys. Rev. B **97**, 035201 (2018).

[39] P. D. Cunningham, K. M. Mccreary, and B. T. Jonker, J. Phys. Chem. Lett. **7**, 5242 (2016).

[40] M. Palummo, M. Bernardi, and J. C. Grossman, Nano Lett. **15**, 2794 (2015).

[41] G. Aivazian, H. Yu, S. Wu, J. Yan, D. G. Mandrus, D. Cobden, and W. Yao, 2D Mater. **4**, 025024 (2017).

[42] P. D. Cunningham, A. T. Hanbicki, K. M. McCreary, and B. T. Jonker, ACS Nano **11**, 12601 (2017).

[43] E. A. A. Pogna, M. Marsili, D. De Fazio, S. Dal Conte, C. Manzoni, D. Sangalli, D. Yoon, A. Lombardo, A. C. Ferrari, A. Marini, G. Cerullo, and D. Prezzi, ACS Nano **10**, 1182 (2016).

[44] S. Gao and L. Yang, Phys. Rev. B **96**, 155410 (2017).